

Optimization of Interdigitated Electrodes in Electric Field Distribution and Thermal Effect

S. Ismail, N. H. Mahmood and M. A. Abdul Razak

Department of Electronics & Computer Engineering, Faculty of Electrical Engineering, Universiti Teknologi Malaysia,
81310 UTM Johor Bahru, Malaysia.
mohdazhar@utm.my

Abstract—Microfluidic is used to separate, transport and manipulate particles through a micro-scale device. This paper presents the numerical simulation of interdigitated electrodes that is commonly used for continuous particle separation using electrical separation microfluidic device which demonstrates dielectrophoretic (DEP) force. The strength of DEP force depends on the gradient of electric field generated by the electrodes. Besides, the effect of Joule heating generated by the electrodes would harm the living particles. The interdigitated electrodes arrays are simulated using COMSOL Multiphysics 3.5. The gradient of electric field distribution and temperature generated are simulated for different width and gap of the electrode. The simulation results are analysed and discussed to determine the best electrode dimension to be fabricated for bio-particles separation application. The optimum interdigitated electrode dimension identified in this research was 60 μm :180 μm (width:gap) that generate $1.92 \times 10^{16} \text{ V}^2\text{m}^{-3}$ of electric field gradient and temperature of 68 $^\circ\text{C}$ on the electrode surface, and electric field gradient of $1.83 \times 10^{13} \text{ V}^2\text{m}^{-3}$ and temperature about 40 $^\circ\text{C}$ when 80 μm above the electrode with the conductivity of the fluid is 1.09 S/m (mimic blood conductivity).

Index Terms—Dielectrophoretic; Electric Field; Joule Heating; Microfluidic.

I. INTRODUCTION

Microfluidics has become one of the interesting investigations in this era since it has shown rapid advances in developing it [1]. Microfluidic is a device that can transport and manipulate small (micro- and smaller) particles through a small dimension of channels [2]. This device is not a new science but it is currently developing to become more modern technology. Microfluidics is a lab-on-a-chip device which is fabricated by Micro-Electro-Mechanical Systems (MEMS) technology. Numerous tasks can be done using this small chip, such as mixing, separating, driving fluids, and analysing and detecting molecules [3]. One of the application of microfluidic is to separate micro particles which is essential in the biomedical field particularly in diagnosing and analysing disease [4], [5]. There is a need of this technology in the medical field so that if a particle can be diagnosed, for example cancer cells, it can be treated at the early stage.

Different kinds of separation techniques have been developed recently [4], such as optical separation [6], magnetic separation [7], electrical separation [8], fluidic-only separation [9] and other separation which are, thermal fractionation [10] and acoustic fractionation [11]. This paper focuses more on electrical separation that demonstrates dielectrophoretic (DEP) forces acting on a planar

microelectrode. There are two types of microelectrode design to manipulate microparticles, namely 2-Dimensional (2D) and 3-Dimensional (3D) microelectrode. Most microfluidic devices are employing 3D microelectrodes due to well distributed electric field [12]. Nevertheless, 3D is hard to fabricate compared to 2D planar electrodes. Metal electroplating technique can be used, but it requires a high aspect ratio and the procedures are complicated [13].

Whenever there is an electrical current flow through a conductive media, heat is generated known as Joule heating. It is also known as resistive heating where it is a volumetric heating which give rise to an electrothermal flow (ETF) [14]. ETF is a common occurrence in electrohydrodynamics, caused by electrothermal forces acting upon a fluid with the presence of electrical conductivity and permittivity in an electrolyte solution [15]. According to Yan *et al.* [16], the heat produced by the conductive media is directly proportional to the square of electric field distribution. This paper presents the analysis of electric field gradient distribution and electrothermal generated by the different ratio of interdigitated electrodes. The simulation software used in this research is COMSOL Multiphysics 3.5. From the simulation, the optimum dimension of the interdigitated electrode is identified to be used for trapping particles using dielectrophoresis technique.

II. LITERATURE REVIEW

A. Dielectrophoretic Force

Dielectrophoresis is a term introduced by Pohl in 1960 which describes the motion of microscopic sized particle produced by the net body force based on the electrical polarizability [1]. In other words, DEP refers to the interaction between the motion of a particle and a non-uniform electric field applied to it [17-19]. DEP is one of the most chosen methods to separate and manipulate particles rather than other separation techniques [17] because it does not require fluorescent, luminescent or radioactive probes as markers and labels to study the behaviour of a particle [18].

The time-averaged force acting on the particle with radius r in AC electric field is calculated using Equation (1) [17-22];

$$F_{\text{DEP}} = 2\pi r^3 \text{Re}[\mathbf{K}] \epsilon_m \nabla E^2 \quad (1)$$

where ϵ_m is the permittivity of the surrounding medium, ∇E^2 represents the gradient of the square electric field which is defined as:

$$\nabla E^2 = \frac{\partial^2 E^2}{\partial x^2} \hat{x} + \frac{\partial^2 E^2}{\partial y^2} \hat{y} + \frac{\partial^2 E^2}{\partial z^2} \hat{z} \quad (2)$$

and $\text{Re}[\mathbf{K}]$ is the real part of Clausius-Mossotti factor. $[\mathbf{K}]$ is defined as:

$$[\mathbf{K}] = \frac{\epsilon_{particle}^* - \epsilon_m^*}{\epsilon_{particle}^* + \epsilon_m^*} \quad (3)$$

where $\epsilon_{particle}^*$ is the complex permittivity of the particle and ϵ_m^* is the complex permittivity of the medium. The factor $\text{Re}[\mathbf{K}]$ is either in negative or positive value [23]. It is said that when the particle is less polarizable than the surrounding medium ($\text{Re}[\mathbf{K}] < 0$), negative DEP (nDEP) takes place [17,19]. In contrary, when particle is more polarizable than the surrounding medium ($\text{Re}[\mathbf{K}] > 0$), positive DEP (pDEP) pulls the particle towards the electrodes.

B. Thermal effects

Joule heating affects the temperature whenever there is an electric field produce by the electrodes [24]. The materials parameters that affect changes of temperature are conductivity, permittivity, density and viscosity of the medium, and diffusion coefficient of particles [15, 25]. The following Laplace equation is used to solve the electric field [15]:

$$\nabla^2 V = 0 \quad (4)$$

where V is the root mean square voltage and the resultant electric field is

$$\mathbf{E} = -\nabla V \quad (5)$$

Then, Equation (6) is used to solve the energy conservation equation which is expressed as [25]

$$\rho c_p \left(\frac{\partial T}{\partial t} + \mathbf{u} \cdot \nabla T \right) = \nabla \cdot (k \nabla T) + \langle \sigma E^2 \rangle \quad (6)$$

where ρ is the density, c_p represents the specific heat, T is the temperature, \mathbf{u} is the velocity, k is the thermal conductivity of the fluid, σ represent the electrical conductivity of the fluid. The term $\langle \sigma E^2 \rangle$ denotes the time averaged Joule heating [26].

Based on Boika and Baranski, strong electric field does not only affect electrothermal convection but also increases the dielectrophoretic force which can be analysed more [27]. Ramos et al. stated that low conductivity solutions produce a little rise of temperature which can be neglected, for example the conductivity of 0.01 S/m with applied potential of 10V give a temperature rise of 1° [28]. The increase of nonuniform electric field and electrothermal generated is caused by the geometry of the electrodes [29]. Warnt *et al.* found out that an increase in temperature would affect the cell in terms of shape and structural change [30]. Warnt *et al.* claimed that thermal heating would significantly affect the cell nuclei where the DNA double strand starts to melt at 70°C while the cell shape starts to change between 42 to 48°C. At 50°C the cell starts to undergo cell death but the nuclei structure is still maintained. However, at 54°C, the nuclei lose their function.

III. METHODOLOGY

The method used in this research is a numerical simulation. The Finite Element Modelling software used to simulate the performance of planar microelectrodes is COMSOL Multiphysics 3.5. First simulation is to determine which electrode ratio (width:gap) produces the optimum electric field distribution while the second simulation is to determine which ratio generates lower temperature that is suitable to be used in a microfluidic device to trap cells.

A. Electric Field Distribution Simulation

The simulation is performed to observe which dimensions generate better electric field. Multiphysics Electrostatic (emes) and Conductive Media DC (emdc) are chosen for the simulation. Figure 1 illustrates the microfluidic channel with interdigitated electrode arrays. The boundary of the electrode is set to 10V and -10V as shown in Figure 2. Only two electrodes in half width and a gap are simulated due to symmetrical of the electrodes. The height of the microfluidic channel is set to be 100µm and the typical thickness of the electrode is 15µm [30].

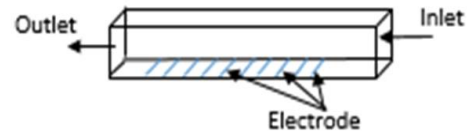


Figure 1: Microfluidic channel with interdigitated electrode arrays

The dimension of the electrode is drawn according to 1:1 (width:gap) ratio, which means the width of the electrodes is similar with the gap between the electrodes. The dimensions are varied from 20µm:20µm to 40µm:40µm, 60µm:60µm, 80µm:80µm, and 100µm:100µm. From the ratio 1:1 results, the ratio that generates and penetrates high electric field is then varied to 1:2 and 1:3 (width:gap) ratio. The electric field distribution and temperature generated are recorded and plotted at different height across the microfluidic channel.

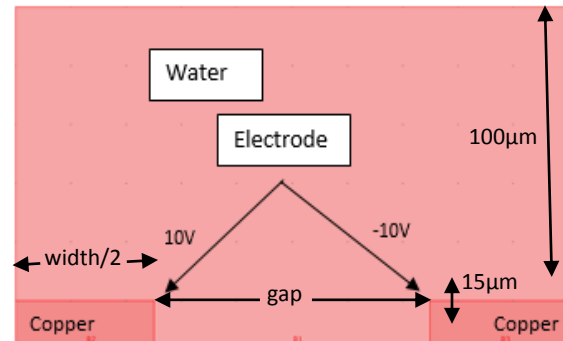


Figure 2: Subdomain and boundary setting of geometry drawn in COMSOL Multiphysics for electric field simulation

Refine meshing is performed to subdivide the geometry into smaller domains called elements. As these elements are made smaller and smaller, the computed solution will approach the true solution. Finer meshing can produce a better result, but a larger storage is needed to store the solution. The result of the simulation is viewed by choosing the parameters in post-processing section. The gradient of electric field is viewed and plotted using Equation (2).

B. Heat Transfer Simulation

The simulation of heat transfer is similar to electric field distribution, but the multiphysics chosen are General Heat Transfer (htgh) and Conductive Media DC (emdc). The electrode dimension is similar to the electric field simulation.

Based on Liu *et al.* [26], the temperature reference value T_0 is set to 300.15K or 26.85°C. The boundaries for the upper and lower microfluidic device are defined to be natural horizontal plane while both side boundaries are defined to be natural vertical wall as shown in Figure 3. The boundary of the copper electrode is set to be temperature at 26.85°C. In this simulation, the conductivity of the fluid (σ) is set to 0.0575 S/m [31].

Once the domains and boundaries of the electrodes are defined, fine meshing is performed and the temperature is computed using Equation (6). Then, the conductivity is changed to 1.09 S/m that mimic conductivity of blood [32]. The simulation is repeated for a different ratio of electrodes namely 1:2 and 1:3 to observe which ratio generate lower temperature.

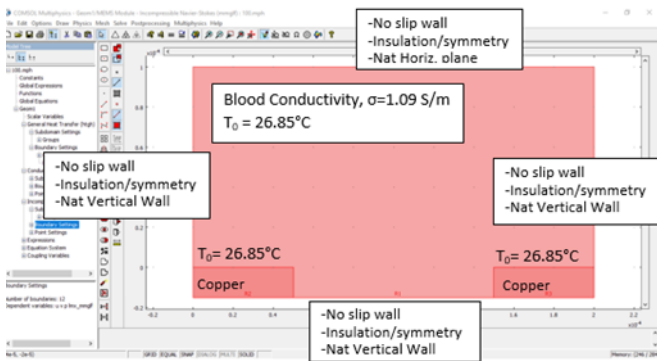


Figure 3: Subdomain and boundary setting of geometry drawn in COMSOL Multiphysics for heat transfer simulation

IV. RESULTS AND DISCUSSION

Two sets of results are presented. The first set of results showed a similar ratio of electrodes width:gap produced gradient of electric field distribution. The second set of results identified different ratio of electrodes width:gap generated the heat within the microfluidic channel.

A. Gradient of Electric Field Distribution

The dimensions described in the methodology were simulated to observe which dimension of interdigitated electrodes generate the highest electric field gradient. Figure 4 shows the graph of the electric field gradient with different electrode width:gap dimension. The electric field gradient was measured on the surface of the electrode

and followed by 20µm, 40µm, 60µm and 80µm above the electrode. Based on the result, the electrode with the gap and width of 20µm generates a higher electric field gradient due to closer electric field lines, but produce rapidly drop in electric field when it is further from the electrode. The other dimensions generate lower electric field gradient at the surface of the electrode but higher electric field gradient when it is 80µm above the electrode as compared to 20µm:20µm. For dimensions of 60µm:60µm, 80µm:80µm and 100µm:100µm, the electric field gradient is considerably high with value ranging from 3.37×10^{13} to $3.90 \times 10^{13} \text{ V}^2\text{m}^{-3}$ at 80µm above the electrode. The field gradient at the electrode surface of 60µm:60µm has higher strength as compared to 80µm:80µm and 100µm:100µm. Based on these comparison, the optimum dimension for 1:1 (width:gap) electrode ratio is 60µm:60µm due to high electric field gradient generated at the surface of the electrode and able to penetrate 80µm away from electrode surface. The simulation was continued by simulating the electrodes ratio of 1:2 and 1:3 (width:gap) using electrodes width of 60µm, and the electric field gradient distribution results are shown in Figure 5.

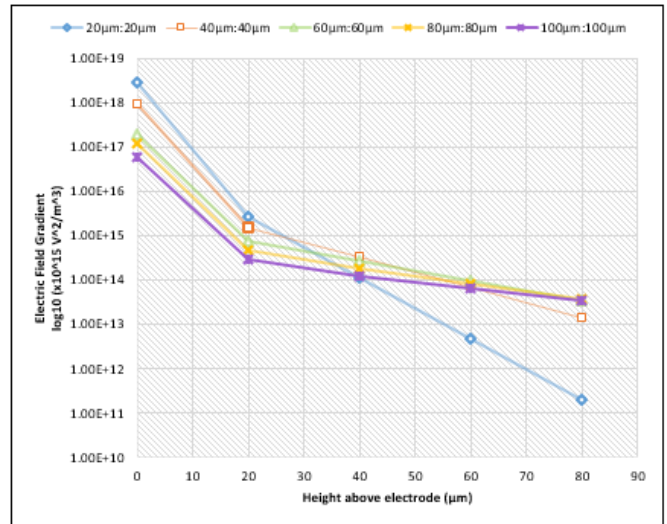


Figure 4: Electric field gradient distribution for different 1:1(width:gap) electrode ratio

From Figure 5, it can be observed that the gradient of electric field distribution for 60µm:60µm is higher than 60µm:120µm and 60µm:180µm due to the smaller gap between two electrodes. Figure 6 shows the result of electric field distribution for electrode with the width of 60µm and the gap of 180µm. The colour bar indicates the level of the electric field which red colour indicates the highest electric field generated while the blue indicates the lowest electric field generated and the arrow shows the direction of the electric field. Also, it can be seen that the edge of the electrode has the highest value of electric field gradient because sharp edges has small area which produce large charge density and electric field distribution.

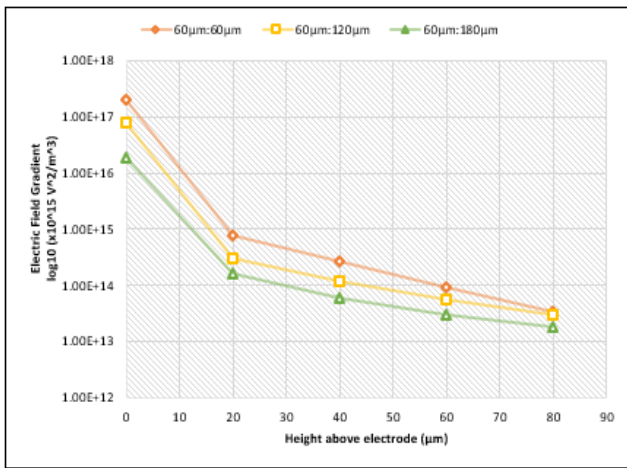


Figure 5: Electric field gradient distribution for different width:gap electrode ratio

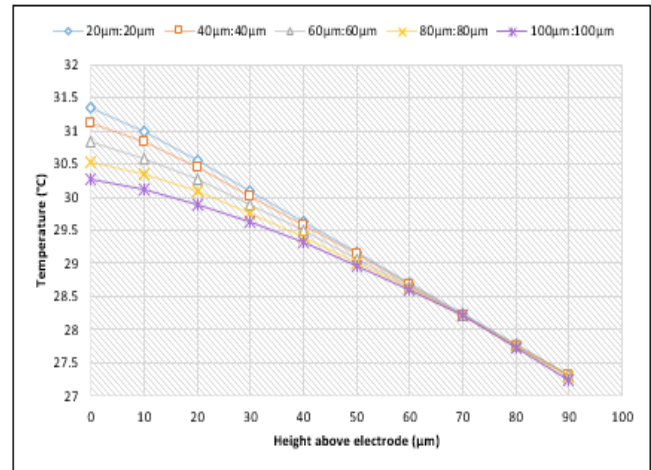


Figure 7: Temperature generated for 1:1 (width:gap) electrode ratio with $\sigma = 0.0575 \text{ S/m}$

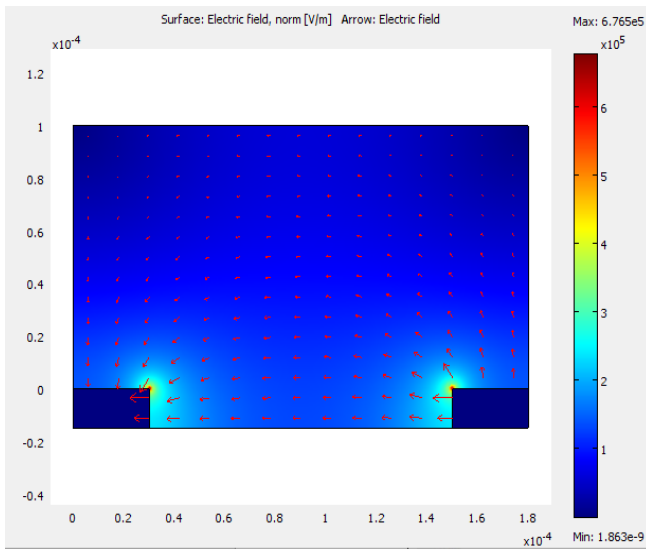


Figure 6: Gradient of electric field for electrode with width:gap ratio of 60μm:180μm

B. Heat Transfer of electrode

As stated in the methodology, the same dimensions of interdigitated electrodes were simulated with the medium conductivity of 0.0575 S/m. The temperature was measured on the surface of the electrode and followed by 10μm, 20μm, 30μm, 40μm, 50μm, 60μm, 70μm, 80μm and 90μm above the electrode. The temperature obtained is plotted and shown in Figure 7. It can be observed that the electrode geometry of 100μm:100μm generates the lowest temperature while the geometry of 20μm:20μm generates the highest temperature. The closer the gap, the higher the heat generated. By increasing the electrode dimension, the temperature generated decreasing. It can be said that the temperature generated is proportional to the electric field produced.

The electrode dimension 60μm:60μm was chosen to vary the gap since it penetrated higher electric field gradient even at 80μm above the electrode. The same method was repeated to observe which dimension generates lower temperature by simulating the electrode width:gap ratio 1:2 and 1:3. The temperature obtained is plotted and shown in Figure 8. It was observed that dimension 60μm:180μm generates lower temperature than 60μm:60μm and 60μm:120μm.

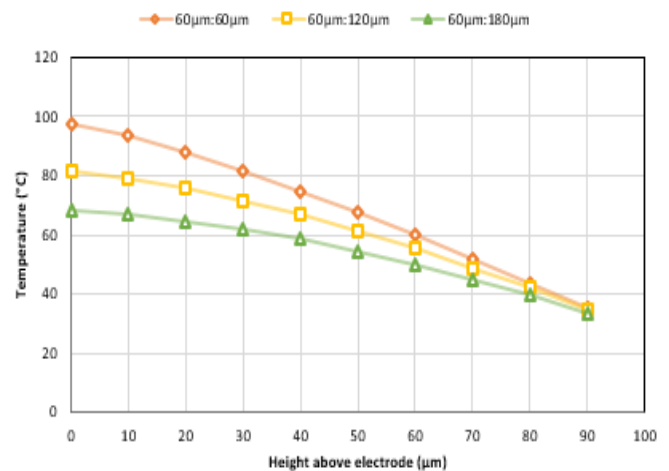


Figure 8: Temperature generated for different electrode ratio with $\sigma = 1.09 \text{ S/m}$

C. Optimization of interdigitated electrodes

Based on the electric field gradient simulation (Figure 4), dimension 20μm:20μm generated higher electric field on the electrode surface, but lower electric field when it is further from the electrode. Increasing dimension could generate slightly lower electric field, but better electric field gradient penetration. Electrode dimension 60μm:60μm, 80μm:80μm and 100μm:100μm produced higher electric field gradient at 80μm above electrodes. However, among these three, electrode dimensions 60μm:60μm generated highest electric field on the electrode surface and almost similar strength at 80μm above electrodes.

For heat transfer, increasing conductivity of medium could cause temperature increases. Based on Figure 8, the temperature generated on the electrode surface is 98°C when electrode dimension is 60µm:60µm. When the gap was increased to 120µm and 180µm, the temperature on the electrode surface decreased to 81.5°C and 68°C respectively. Therefore, the electrode dimension ratio 1:3 was chosen to be the acceptable ratio because it generates considerably lower temperature than ratio 1:1 and 1:2. Moreover, the electrode ratio 1:3 generated better electric field penetration up to 80µm away from the electrode.

V. CONCLUSION

The electric field gradient distribution and the temperature generated by the interdigitated electrodes with different dimension and ratio were numerically simulated and analysed. It can be concluded that the closer the gaps, the higher the electric field and temperature generated by the electrodes. The electric field and temperature decrease when it is further from electrode surface. As for temperature generation, the higher the electrolyte conductivity, the higher the temperature generated by the interdigitated electrodes. When the conductivity of the medium was changed from = 0.0575 S/m to 1.09 S/m, the temperature above the electrode increased up to 70% for 1:1 (width:gap) electrode ratio. The electrode dimension of 60µm:180µm was chosen to be the optimum ratio for particle trapping because it generates considerably high electric field about $1.92 \times 10^{13} \text{ V}^2\text{m}^{-3}$ at 80µm from the electrode surface. The higher electric field is needed so it can push or attract particles acting on the electrode during the particle separation and low temperature generated is important so that it would not harm the living particles.

ACKNOWLEDGMENT

This work is supported by the Universiti Teknologi Malaysia (UTM) under the Research University Grant (GUP) (Q.J130000.2623.14J23).

REFERENCES

- [1] Y. Li, C. Dalton, H. Crabtree, G. Nilsson and K. Kaler, "Continuous dielectrophoretic cell separation microfluidic device," *The Royal Society of Chemistry*, pp. 239-248, 2006.
- [2] G. M. Whitesides, "The origins and the future of microfluidics," *Nature*, pp. 368-373, 2006.
- [3] I.S. Jacobs and C.P. Bean, "Fine particles, thin films and exchange anisotropy," in *Magnetism*, vol. 3, G.T. Rado and H. Suhl, Eds. New York: Academic, 1963, pp. 271-350.
- [4] P. Tabeling, "Some basic problems of microfluidics," in *14th Australasian Fluid Mechanics Conference*, Adelaide, 2001, pp. 57-62.
- [5] H. Stone and S. Kim, "Microfluidics: Basic Issues, Application, and Challenges," *AIChE Journal*, vol. 47, no. 6, pp.1250-1254, 2001.
- [6] M. Macdonald, G. Spalding and K. Dholakia, "Microfluidic sorting in an optical lattice," *Nature*, pp. 421-424, 2003.
- [7] N. Pamme, "Magnetism and microfluidics," *Lab Chip*, pp. 24-38, 2006.
- [8] F. Baldessari and J. Santiago, "Electrophoresis in nanochannels: brief review and speculation," *J. Nanobiotechnol*, pp. 189-195, 2006.
- [9] M. Yamada, M. Nakashima and M. Seki, "Pinched flow fractionation: continuous size separation of particles utilizing a laminar flow profile in a pinched microchannel," *Analytical Chemistry*, pp. 5465-5471, 2004.
- [10] T. Edwards, B. Gale and A. Frazier, "A microfabricated thermal field-flow fractionation system," *Analytical Chemistry*, pp. 1211-1216, 2002.
- [11] A. Nilsson, F. Petersson and H. Jonsson, "Acoustic control of suspended particles in micro fluidic chips," *Lab Chip*, pp. 131-135, 2004.
- [12] D. Chen, H. Du, H. Gong and W. Li, "A 3-D Microelectrode System for Dielectrophoretic Manipulation of Microparticles," *Journal of Physics: Conference Series*, pp. 1008-1013, 2006.
- [13] S. Lee, G. Y. Yun, Y. Koh, S. H. Lee and Y. K. Kim, "Fabrication of a 3 dimensional dielectrophoresis electrode by a metal inkjet printing method," *Micro and Nano System Letters*, pp. 1-7, 2013.
- [14] G. Y. Tang, D. G. Yan, C. Yang, H. Q. Gong, C. J. Chai and Y. Lam, "Joule heating and its effects on electroosmotic flow in microfluidic channels," *Journal of Physics: Conference Series*, pp. 925-930, 2006.
- [15] F. Hong, J. Cao and P. Cheng, "A parametric study of AC electrothermal flow in microchannels with asymmetrical interdigitated electrodes," *International Communications in Heat and Mass Transfer*, pp. 275-279, 2011.
- [16] Y. Yan, D. Guo and S. Wen, "Joule heating effects on two-phase flows in dielectrophoresis microchips," *BioChip J.*, pp. 1-10, 2017.
- [17] N. Lewpiriyawong, K. Kandaswamy, C. Yang, V. Ivanov and R. Stocker, "microfluidic characterization and continuous separation of cells and particles using conducting poly(dimethyl siloxane) electrode induced alternating current-dielectrophoresis," *Analytical Chemistry*, pp. 9579-9585, 2011.
- [18] D. Lee, B. Hwang and B. Kim, "The potential of a dielectrophoresis activated cell sorter (DACS) as a next generation cell sorter," *Micro and Nano Systems Letter*, pp. 1-10, 2016.
- [19] Y. Zhao and L. Zheng, "A simple and quick fabrication method of microfluidic cell sorter using dielectrophoresis," in *2013 IEEE 7th International Conference on Nano/Molecular Medicine and Engineering (NANOMED)*, Thailand, 2013, pp.32-35.
- [20] N. Yunus, Z. Abidin and I. Halin, "Characterization of microelectrode array of dielectrophoretic microfluidic device," *Journal of Bioengineering & Biomedical Science*, pp. 1-8, 2016.
- [21] Z. Zhao, X. Zheng, J. Yang, X. Wu, X. Hei and Y. Cao, "Dielectrophoretic Manipulation of cells by Using Interdigitated Microelectrodes," in *1st IEEE International Conference on Nano/Micro Engineered and Molecular Systems, 2006 (NEMS'06)*, China, 2006, pp. 1021-1024.
- [22] E. Kurgan and P. Gas, "An influence of electrode geometry on particle forces in ac dielectrophoresis," *Electrical Review*, pp. 103-105, 2010.
- [23] S. Hu, Y. Zhao and H. Hu, "modeling and simulation of tapered fiber-optic oil concentration sensor using negative dielectrophoresis," *Sensors and Actuators B: Chemical*, pp. 70-75, 2014.
- [24] O. T. Nedelcu, "A Thermal Study on Joule-Heating Induced Effects in Dielectrophoretic Microfilters," *Romanian Journal of Information Science and Technology*, pp. 309-323, 2011.
- [25] S. Park, M. Koklu and A. Beskok, "Particle Trapping in high conductivity media with electrothermally enhanced negative dielectrophoresis," *Analytical chemistry*, vol. 81, no. 6, pp. 2303-2310, 2009.
- [26] W. Liu, Y. Ren, J. Shao, H. Jiang, and Y. Ding, "A theoretical and numerical investigation of travelling wave induction micrfluidic pumping in a temperature gradient," *Journal of Physics D: Applied Physics*, pp. 1-15, 2014.
- [27] A. Boika and A. S. Baranski, " Dielectrophoretic and electrothermal effects at alternating current heated disk microelectrodes," *Analytical Chemistry*, pp. 7392-7400, 2008.
- [28] A. Ramos, H. Morgan, N. Green and A. Castellanos, "Ac Electrokinetics: A review of forces in microelectrode structures," *Journal of Physics D: Applied Physics*, pp. 2338-2353, 1998.
- [29] B. Shaparenko, "The Thermal Dielectrophoretic Force on a Dielectric Particle in Electric and Temperature Fields," *Phd Thesis*, University of Pennsylvania, United States, 2015.
- [30] J. Song, Y. Liao, C. Liu, D. Lin, L. Qiao, Y. Cheng, S. Koji, M. Katsumi and S. Zhang, "Fabrication of Gold Microelectrodes on a Glass Substrate Femtosecond-Laser-Assisted Electrode Plating," *Journal of Laser Micro/Nanoengineering*, vol. 7, pp. 334-338, 2012.
- [31] N. Gunda, S. Bhattacharjee and S. Mitra, "Study on the use of dielectrophoresis and electrothermal forces to produce on-chip micromixers and microconcentrators," *Biomicrofluidics*, pp. 1-23, 2012.
- [32] S. Abdalla, S. Al-ameer and S. Al-Mahaishi, "Electrical Properties with relaxation through human blood," *Biomicrofluidics*, pp.1-16, 2010.